INTERNATIONAL JOURNAL OF CLIMATOLOGY
Int. J. Climatol. **30**: 359–371 (2010)
Published online 30 March 2009 in Wiley InterScience
(www.interscience.wiley.com) DOI: 10.1002/joc.1902

RMetS
Royal Meteorological Society

Impacts of Pacific and Indian Ocean coupling on wintertime tropical intraseasonal oscillation: a basin-coupling CGCM study

Shu-Ping Weng[a]* and Jin-Yi Yu[b]
[a] *Department of Geography, National Taiwan Normal University, Taipei, Taiwan*
[b] *Department of Earth System Science, University of California, Irvine, USA*

ABSTRACT: This study examines the respective influences of Pacific and Indian Ocean couplings on tropical intraseasonal oscillation (ISO) in boreal winter (November–April). Three basin-coupling experiments are performed with a coupled atmosphere-ocean general circulation model (CGCM), in which air-sea coupling is limited respectively to the Indian Ocean, the Pacific Ocean, and both the oceans. The modelling results show that zonal ISO propagations can be found in the Indo-Pacific region with or without the ocean coupling; however, the propagation signals are enhanced by the coupling. In this particular model the Pacific Ocean coupling has a stronger influence on the ISO propagation than the Indian Ocean coupling. Without the Pacific coupling, the ISO propagation signal is weakened significantly when it enters the Pacific Ocean sector. Without the Indian Ocean coupling, the simulated ISO intensity is weakened less in the Indain Ocean, and significant zonal propagations of ISO can still be simulated in the sector. The relative importance of the ocean coupling is likely related to the smaller ISO-related sea surface temperature (SST) anomalies in the Indian Ocean than in the Pacific Ocean. In this particular CGCM, the ocean coupling affects the ISO propagation mainly through a wind-evaporation-SST feedback rather than a cloud-radiation-SST feedback, while in observations both processes are equally important. To further confirm the importance of the ocean coupling, forced atmospheric GCM experiments are performed with SSTs prescribed from the climatologies produced in the basin-coupling experiments. It is found that the eastward propagating feature seen in the CGCM experiments is weakened and dominated by the strong standing feature in the forced AGCM runs. The difference demonstrates the contribution of the ocean coupling to the ISO propagation, and also confirm that biases in the mean SST and low-level wind caused by the ocean coupling are responsible for the spurious standing ISO oscillation feature in the central Pacific and Indian Oceans. Copyright © 2009 Royal Meteorological Society

KEY WORDS intraseasonal oscillation; atmosphere-ocean coupling; Madden–Julian oscillation; Indo-Pacific climate variability

Received 13 February 2008; Revised 4 September 2008; Accepted 3 March 2009

1. Introduction

Since the pioneering work of Madden and Julian (1971, 1972), tropical intraseasonal oscillation (ISO) has been increasingly recognized as a phenomenon important to both climate and weather. This phenomenon is characterized by large-scale convection and circulation anomalies, propagating primarily eastward along the equator and with broad timescales of 20–90 days. Observational studies have revealed that intraseasonal fluctuations also occur in sea surface temperature (SST) in association with the passage of ISO in the Indo-Pacific warm pool (e.g. Krishnamurti *et al*., 1988; Zhang, 1996, 1997; Weller and Anderson, 1996; Lau and Sui, 1997; Hendon and Glick, 1997; Woolnough *et al*., 2000). The coherent fluctuations between ISO and SST have prompted the notion that the atmosphere-ocean coupling is an important ingredient for the tropical ISO dynamics (e.g. Wang, 2005).

Coupled atmosphere-ocean models with various complexities had been used to study the importance of the ocean coupling to ISO. The results have not been conclusive and appear model dependent. However, many studies found that the coupling enables the employed models to produce more realistic ISO, indicating the importance of the coupling to the ISO simulation. Wang and Xie (1998) coupled a simple atmospheric model to a mixed-layer ocean and showed that intraseasonal SST variations can affect surface pressure and thus enhance or reduce ISO convective activity. They argued that the coupling could destabilize the atmosphere for the growth of ISO. The coupling also slows down the propagation speed and allows their simple coupled model to produce more realistic ISO. Waliser *et al*. (1999) coupled a slab ocean model to the Goddard Laboratory for the Atmospheres (GLA) GCM and also found the ocean coupling improves the ISO simulations. Watterson (2002) used the CSIRO Mark2 coupled atmosphere-ocean general circulation model (CGCM) to examine the sensitivity of ISO to model ocean configurations. His results showed that

* Correspondence to: Shu-Ping Weng, Department of Geography, National Taiwan Normal University, Taipei, Taiwan.
E-mail: znspw302@ntnu.edu.tw

the coupling affects the amplitude and propagating speed of the model ISO. With a fully coupled HadCM3 CGCM, Inness and Slingo (2003) showed that many observed ISO features can be captured in the coupled simulation but not in the uncoupled atmosphere-only general circulation model (AGCM) run prescribed with observed SSTs. Fu and Wang (2004) further demonstrated the importance of SST feedback to the ISO evolutions. They coupled the ECHAM4 AGCM to an intermediate ocean model and showed that this hybrid-coupled model can produce realistic propagating ISO. But when they forced the same AGCM with the simulated SST produced from the coupled run, the model produces erroneous standing oscillation. Zhang *et al*. (2006) performed several pairs of CGCM and AGCM experiments to show that the ocean coupling generally strengthens the simulated propagating ISO signal. Recently, Watterson and Syktus (2007) further found the responsiveness of model mixed layer in the Pacific warm pool crucial for providing a sufficient SST response to help the ISO propagate through the Maritime Continent into the western Pacific.

One issue not addressed in these coupled modelling studies is the individual roles of the Pacific and Indian Ocean couplings to the propagation of ISO. Observations showed that, in boreal winter, the ISO propagation is predominantly eastward after being initiated in the western Indian Ocean. It then passes through the Maritime Continent, redevelops over the western Pacific warm pool, and often intersects the South Pacific convergent zone (SPCZ) where the warm SSTs reside (Wang and Rui, 1990; Jones *et al*., 2004). The path of the ISO propagation was noticed to be more or less in accord with the warm SST ($>27\,^{\circ}$C) distribution. Figure 1(a) shows that winter (November–April; NDJFMA) SST climatology (1981–2001) calculated from NOAA optimum interpolation SST (OISST_v2; Reynolds *et al*., 2002). It is noticed that although the warm SSTs cover both the Indian and Pacific Ocean, the major part of the warm pool is located in the western Pacific Ocean and tends to be less symmetric to the equator as compared to the warm water in the eastern Indian Ocean. The zonal SST gradients are also opposite between the Indian and Pacific Ocean, which are accompanied with opposite cells of Walker circulation. It is also known that surface winds in most of the Pacific Ocean are easterlies but are westerlies in the Indian Ocean. Could the different mean SST and wind distributions in these two ocean basins affect the role of the ocean coupling to the ISO propagation?

To examine this hypothesis, this study contrasts the ISO simulations produced from a series of three basin-coupling CGCM experiments in which the atmosphere-ocean coupling is limited, respectively, to the tropical Pacific Ocean, tropical Indian Ocean and both the tropical Pacific and Indian oceans. In addition to the atmosphere-ocean coupling, the basic state biases in coupled models also affect the ISO simulation (Inness and Slingo, 2003; Zhang *et al*., 2006; Watterson and Syktus, 2007). To separate the effects of atmosphere-ocean coupling and basic state bias on ISO simulations in the CGCM

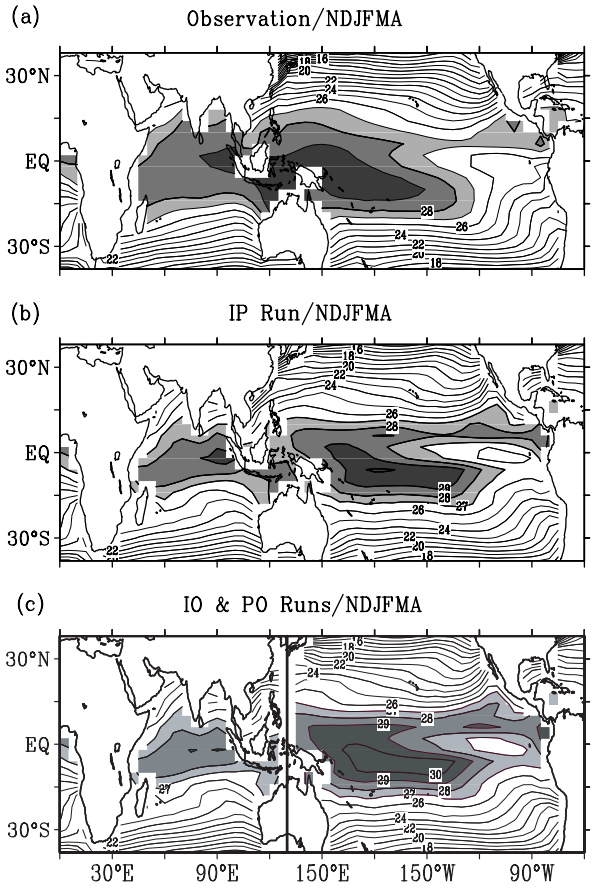

Figure 1. Boreal winter (November–April; NDJFMA) SST climatology calculated from (a) NOAA OISST_v2 dataset (1981–2001), (b) the Indo-Pacific (IP) CGCM, and (c) Indian Ocean (IO; west of 130 °E) and Pacific Ocean (PO; east of 130 °E) CGCM Runs. Contour intervals are 1 °C. This figure is available in colour online at www.interscience.wiley.com/ijoc

experiments, we also performed a series of forced AGCM experiments in which the SSTs are prescribed with the monthly climatologies produced by the basin-coupling CGCM experiments.

This paper is organized as follows. The basin-coupling methodology and the CGCM used in this study are described in Section 2. The simulated ISOs in different experiments are contrasted with the observations in Section 3. The mechanism that allows the ocean coupling to affect the ISO propagation is discussed in Section 4. Results of the forced AGCM runs are also contrasted with their coupled counterparts in this section. Section 5 summarizes the major findings of this study.

2. Model and basin-coupling experiments

The CGCM (detailed in Yu and Mechoso, 2001) used in this study consists of the UCLA AGCM (Mechoso *et al*., 2000) and GFDL Modular Ocean Model (MOM; Bryan, 1969; Cox, 1984). The AGCM component has a global coverage with a horizontal resolution of 4° in latitude and 5° in longitude and 15 levels in the vertical with the top at 1-mb. The oceanic general circulation model (OGCM)

component has a longitudinal resolution of 1° and a latitudinal resolution varying gradually from 1/3° between 10 °S and 10°N to about 3° at both 30 °S and 50°N. It has 27 layers in the vertical with a 10-m resolution in the upper 100 m. The AGCM and OGCM are coupled daily without flux correction. The three basin-coupling experiments we performed are the Pacific Ocean (PO) Run, the Indian Ocean (IO) Run, and the Indo-Pacific (IP) Run. In the PO Run, CGCM includes only the Pacific Ocean (30 °S–50°N, 130 °E–70 °W) in its ocean model domain. The IO Run includes only the Indian Ocean (30 °S–50 °N, 30°–130 °E), whereas the IP Run includes both the Indian and Pacific oceans (30 °S–50 °N, 30 °E–70 °W). Outside the interactive ocean model domains, climatological monthly-mean SSTs are prescribed. Inside the ocean model domains, SSTs poleward of 20 °S and 30°N are relaxed toward their observed climatological values. Therefore, the effectively coupling regions in these CGCM runs are limited to the tropical Pacific and Indian Oceans. The IP, PO, and IO Runs were all integrated for 60 years. Only the daily outputs from the last 30 years of the integrations are analyzed in this study. The observed ISO properties in circulation and convection fields are derived respectively from the daily-mean European reanalysis product ((ERA-40); Uppala *et al*., 2005) and the pentad-mean CPC merged analysis of precipitation ((CMAP); Xie and Arkin, 1997) in their overlapped period of 1979–2001.

The simulated winter-mean SSTs from the three CGCM runs are shown in Figure 1 to be compared with the observed one. The figure shows that the general pattern of the observed Indo-Pacific SST distribution (Figure 1(a)) is reasonably captured in the IP Run (Figure 1(b)). The simulated warm pool covers both the western Pacific Ocean and the eastern Indian Ocean. A cold tongue is reproduced in the eastern equatorial Pacific. Nevertheless, model deficiencies exist, which include a warm bias in the eastern Pacific, north of the equator, a too zonal and too eastward extension of the southern branch of western Pacific warm pool, and a cold bias around the Maritime Continent. Also, the simulated Indian Ocean SSTs are colder than the observed. The mean SST distributions produced by the IO and PO Runs (Figure 1(c)) are in general similar to those of the IP Run in their respected ocean basins, though the cold/warm biases in the Indian/Pacific Ocean increase slightly in the IO/PO Run.

3. Simulated ISO activities in CGCM expeirments

To extract ISO signals from observations and the simulations, we adopt the procedure used by Rui and Wang (1990). The mean annual cycle is first removed from daily data to produce daily anomalies. A 3-month running mean anomaly, which estimates the subannual to interannual variation, is then removed from the daily anomaly before computing the 5-day mean pentad anomaly. This band-pass filtering procedure retains intraseasonal variations with timescales ranging from 10 days to 3 months.

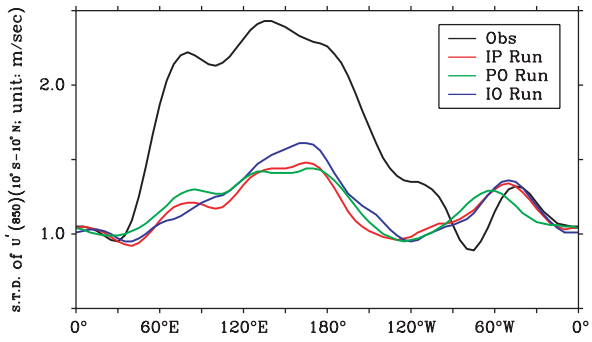

Figure 2. Standard deviations of wintertime bandpass-filtered U'_{850} along the equator (10 °S–10 °N). Black curve is calculated from the observations (ERA-40), red curve from the Indo-Pacific (IP) Run, blue curve from the Indian Ocean (IO) Run, and green curve from the Pacific Ocean (PO) Run. This figure is available in colour online at www.interscience.wiley.com/ijoc

The CMAP dataset is also processed in a similar way but taking its pentad-resolution into account.

Figure 2 compares the variance of the simulated and observed filtered anomalies in 850-mb zonal wind (U'_{850}) averaged between 10 °S and 10°N. In the observations, the ISO variance concentrates in the region from the central Indian Ocean to the west of dateline. The variance decreases rapidly towards the eastern Pacific. The maximum variance appears in the western Pacific warm pool. A secondary maximum occurs in the central Indian Ocean between 60 °E and 90 °E. All the three CGCM experiments produce weaker ISO variances compared to the observed. The peak variances of the simulated ISO in the Pacific and Indian Oceans are about 40–60% of the observed values. Nevertheless, their spatial distributions are in general close to the observed.

To identify the dominant ISO mode and its propagation characteristics, an extended empirical orthogonal function (EEOF) analysis (Weare and Nasstrom, 1982) is applied to the wintertime filtered easterly vertical shear (EVS) anomalies in the tropical eastern hemisphere (20 °S–20 °N, 30 °E–180 °E) where the intraseasonal variance is concentrated. A 5-pentad lead-lagged window is used in the EEOF analysis to portray the evolving ISO signal. Here the EVS is defined as the difference of anomalous zonal winds between 200 mb and 850 mb ($U'_{200} - U'_{850}$). This quantity gives a good measurement of the strength of the gravest baroclinic mode associated with the large-scale deep convections (Wang and Fan, 1999). We find applying the EEOF analysis to the EVS anomalies particularly effective in isolating the ISO from the model experiments where the intraseasonal variability is relatively weak. Choice of this quantity is also in accord with the recent suggestion of Wheeler and Hendon (2004) that ISO is best identified when an EOF analysis is applied to the combined U'_{200}, U'_{850}, and outgoing longwave radiation anomalies together.

The percentages of the 10 to 90-days EVS variance explained by the first pair of EEOF modes for the ERA-40, IP, PO, and IO Runs are, respectively, 27.6, 24.1, 18.3 and 31.3%. Due to the degenerate nature of EEOF

analysis (Fraedrich *et al*., 1997; Hannachi *et al*., 2007), however, the second EEOF mode is redundant having its evolving patterns temporally in-quadrature with those in the first mode. The first EEOF mode from the observed EVS evolution is shown in Figure 3. In Figure 3, a convergent (divergent) zone in the 850-mb level is denoted as the zero contour line of EVS with positive (negative) anomalies to its right and negative (positive) anomalies to its left. The figure shows that the leading ISO mode is characterized by a wavenumber-1 pattern with its convergence/divergence centre propagating eastward along the equator. The wavenumber-1 eastward propagating feature of ISO-related EVS is still captured by the first EEOF mode in the model simulations, although deficiencies mainly exist around the Maritime Continent and southern Indian Ocean (not shown). The lifecycle of ISO is then composited from 40 extreme events (with 20 positive and 20 negative peak events), which were selected based on the principal component of the first EEOF mode. The same procedure is applied to the CGCM experiments to construct the simulated ISO lifecycles.

Figure 4 shows the Hovmöller diagrams of the composite ISO lifecycle in 200-mb velocity potential anomalies (χ'_{200}) along the equator (10 °S–10 °N). The observed χ'_{200} (Figure 4(a)) is characterized by an eastward-propagating wavenumber-1 pattern that circumnavigates the globe in about 50 days. In all the three CGCM runs, the simulated ISOs have smaller amplitudes than observed. A smaller contour interval is used for the simulated χ'_{200} (Figures 4(b)–(d)) than for the observed one. Figure 4(b) shows that the IP Run produces an eastward propagation of ISO that is close to the observation. With the Pacific Ocean coupling but no Indian Ocean coupling, the PO Run (Figure 4(c)) still produces an eastward ISO signal propagating from the Indian Ocean to the Pacific Ocean. With the Indian Ocean coupling but no Pacific Ocean coupling, the intensity of the propagation feature in the IO Run (Figure 4(d)) is strong only in the Indian Ocean. The ISO intensity eastward of the 130 °E is much smaller than that in the Indian Ocean. This is very different from the results of IP and PO Runs, where the ISO intensities in these two regions are comparable. The rapid reduction of the intensity of the propagating ISO suggests that the eastward propagation stalls near 130 °E, which is the eastern boundary of the active Indian Ocean in the IO Run. It should be noted that the IO Run produces the strongest ISO intensity in the Indian Ocean while the PO Run produces the strongest ISO intensity in the Pacific. These modelling results suggest that both the Indian and Pacific Ocean couplings can enhance the intensity of the simulated ISO. However, the ocean coupling in the Pacific Ocean is more crucial to the ISO propagation than that in the Indian Ocean. It is also noticed that the ISO propagation speed in the IO Run is slower than the other runs. Figure 4(a) indicates that the overall propagation speed in the observation is about 7°/day, although the propagation is faster in the western hemisphere than the eastern hemisphere. The propagation speeds are about 5–6°/day in the IP and PO Runs (Figures 4(b) and (c)), close to the observed one. However, in the IO Run, the speed is only about 2–3°/day in the Indian Ocean which is much slower than the observations and the other two CGCM runs. Such a slow down could be due to either the Indian Ocean coupling or the Indian Ocean SST bias produced by the

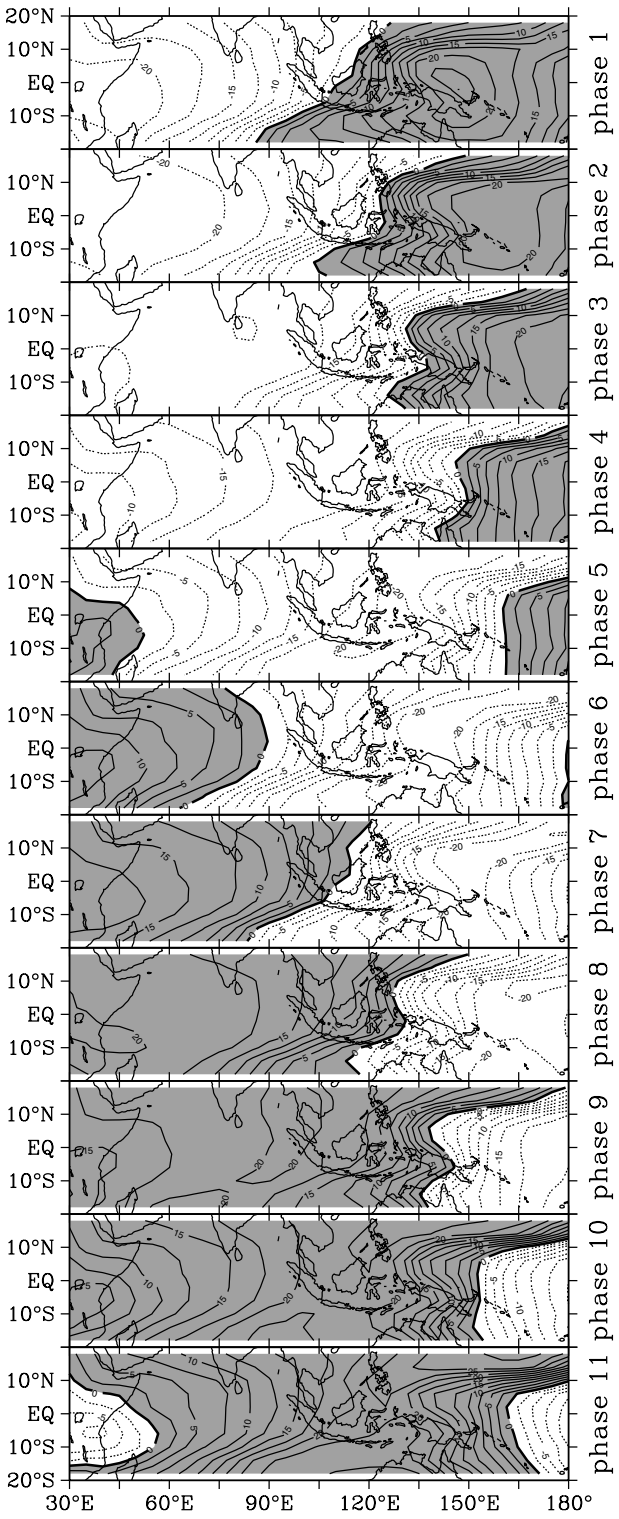

Figure 3. Evolution of the first EEOF mode calculated from the observed easterly vertical shear (EVS) anomalies is shown from phase 1 (−25 days) to phase 11 (+25 day).

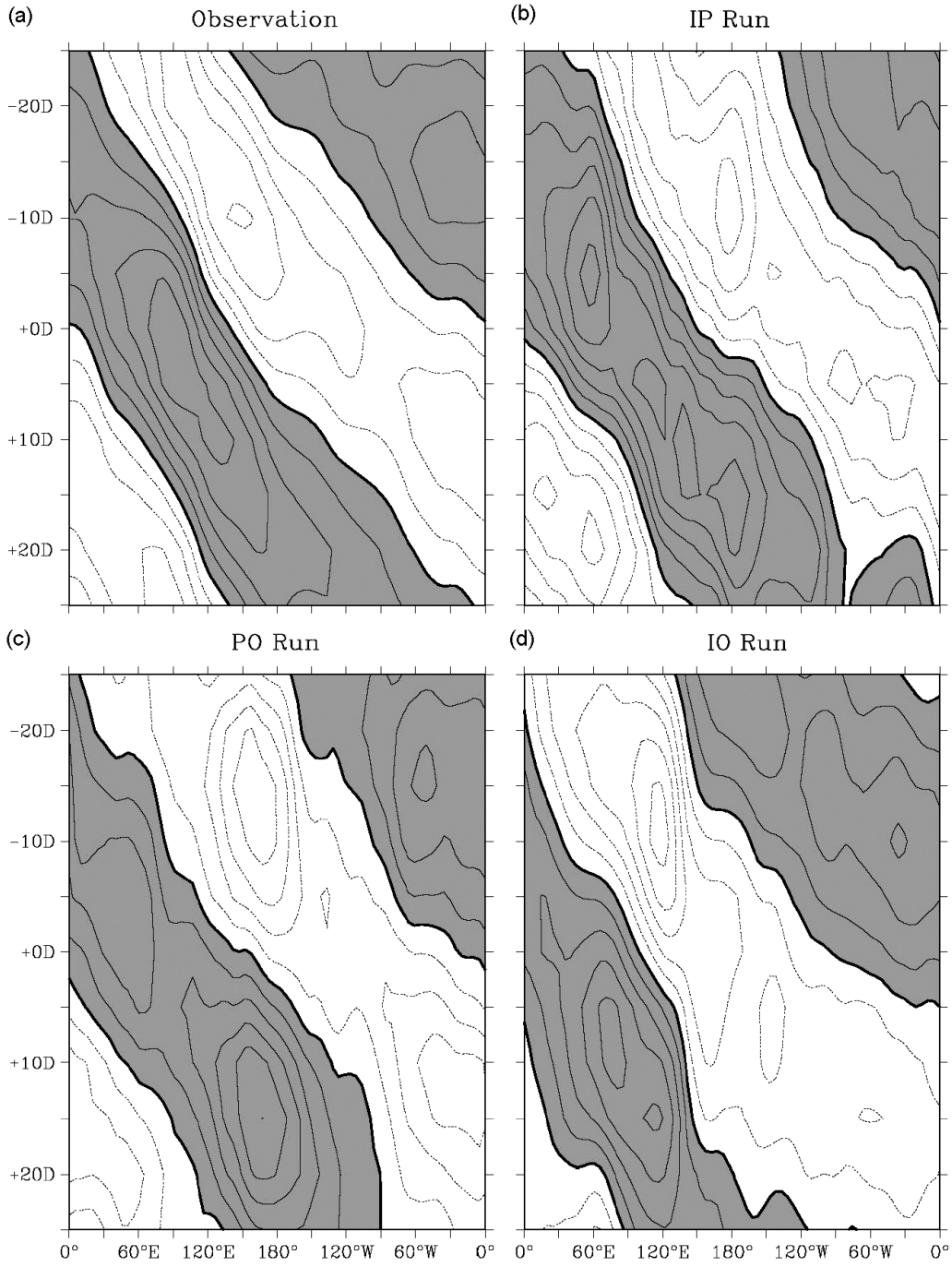

Figure 4. Lifecycle of wintertime ISO in 200-mb velocity potential anomalies (χ'_{200}) along the equator (10 °S–10 °N). Panel (a) is composited from the observations, (b) from the Indo-Pacific (IP) Run, (c) from the Pacific Ocean (PO) Run, and (d) from the Indian Ocean (IO) Run. Contour intervals are 1.0×10^6 m$^2 \cdot$ sec^{-1} in (a) and $1/3 \times 10^6$ m$^2 \cdot$ sec^{-1} in (b)–(d).

coupling. As will be shown and discussed later, the SST bias produces an unrealistically large standing oscillation in the Indian Ocean which may contribute to the reduced ISO propagation speed.

We notice in the IP Run that there are two standing oscillations embedded in the eastward ISO propagation: one is located near 60 °E and the other near 180 °E. Both are manifested as local enhancements of ISO amplitudes. The standing oscillation at 60 °E gets stronger in the IO Run but weaker in the PO Run, whereas the one at 180 °E is the largest in the PO Run but is weak in the IO Run. Results of Figure 4 suggest that these two unrealistic standing oscillations are related to model deficiencies caused by the coupling in the central Indian and Pacific oceans. We notice from Figure 5, which shows the observed and simulated mean wind and velocity potential at 850 mb, that the CGCM runs produce significant biases in the low-level winds near these two regions. In this figure, tropical westerlies are highlighted as red vectors. Figure 5(a) shows that the observed westerlies prevail in the regions between central Indian Ocean and western Pacific warm pool. The IP Run (Figure 5(b)) produces

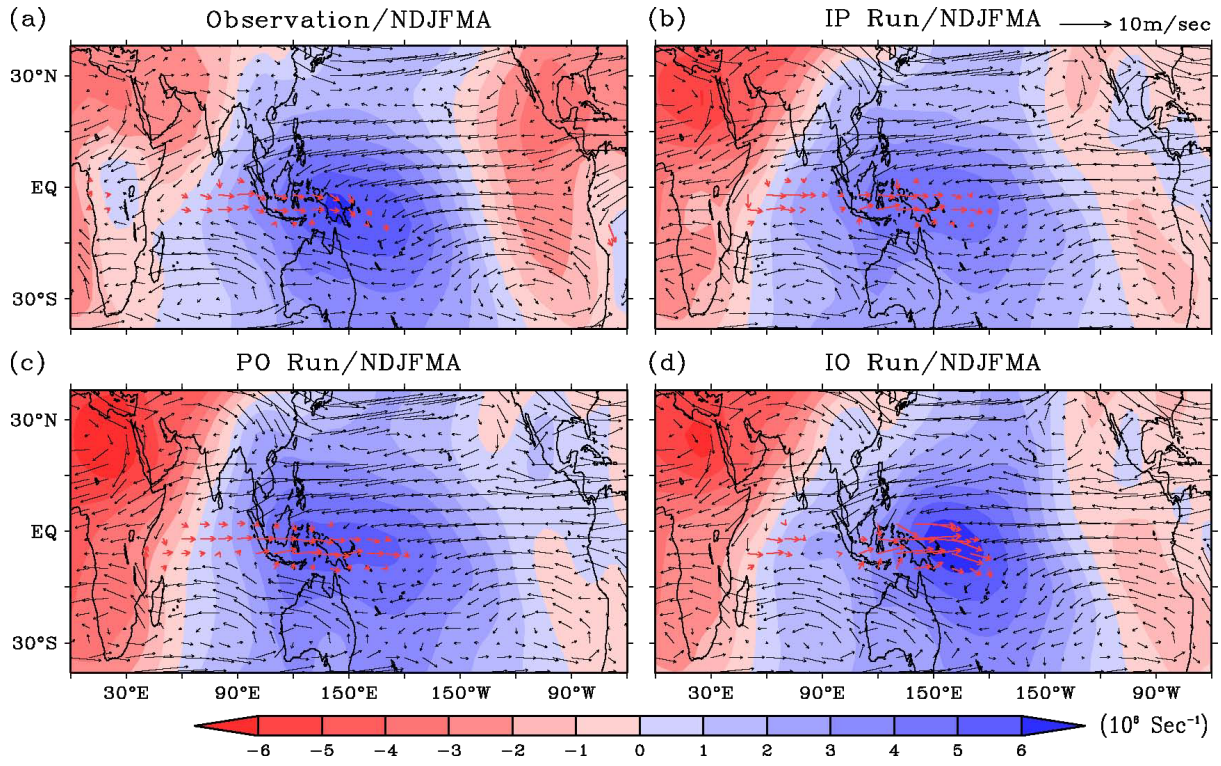

Figure 5. Winter mean 850-mb wind (vector) and velocity potential (contour) calculated from (a) the observation, (b) the Indo-Pacific (IP) Run, (c) the Pacific Ocean (PO) Run, and (d) the Indian Ocean (IO) Run. Tropical westerlies are highlighted red. This figure is available in colour online at www.interscience.wiley.com/ijoc

prevailing westerlies in the regions, similar to those observed. However, the intensity of model westerlies reduces significantly when they approach Sumatra. The westerlies also extend too far eastward and are too strong in the central Pacific. These biases result in unrealistic low-level convergence in the regions close to where the standing ISO oscillations of χ'_{200} are produced. The westerly bias in the Indian Ocean is most serious in the IO Run (Figure 5(d)), in which the westerlies even reverse to easterlies in the eastern Indian Ocean. As mentioned, this run has the most serious standing oscillation at 60 °E among the three runs. The PO Run (Figure 5(c)) does not have a serious wind bias problem in the Indian Ocean; neither did this run produce a large standing oscillation at 60 °E. As for the mean wind bias over the central Pacific Ocean, it occurs in the PO Run but is less obvious in the IO Run because the SSTs therein are prescribed from the observations. This is consistent with the fact that the standing oscillation at 180 °E exists in the PO Run but is weak in the IO Run. Figures 4 and 5 together suggest that the erroneous standing oscillations are caused by the model biases in the mean surface wind simulations. We can further link the wind biases to the SST biases discussed in Figure 1. The cold bias around the Maritime Continent can result in a local high-pressure anomaly from which low-level winds diverge westward and lead to the weakening of the westerlies in the central Indian Ocean. The too-eastward extension of the western Pacific warm pool, on the other hand, enhances and extends the westerlies into the central equatorial Pacific, where they encounter the Pacific easterlies and thereby result in an unrealistic convergence near the dateline.

The zonal propagation of the ISO is further examined in Figure 6 where the observed and simulated ISO lifecycles in rainfall and 850-mb wind anomalies are compared. Only the first half of the lifecycle is shown in the figure. The other half cycle is similar but with an opposite sign. The colour-shaded areas and black vectors denote respectively the rainfall and wind anomalies significant at 95% and 90% confidence levels. The observed (Figure 6(a)) rainfall anomalies show a familiar four-stage development process: (1) initiation over equatorial Africa and/or western Indian Ocean (phase 2) (2) rapid intensification when passing through the Indian Ocean (phases 1–3) (3) mature evolution characterized by a weakening in the Maritime Continent and redevelopment over the western Pacific (phase 3–5) and (4) dissipation when approaching the dateline (phase 6). Associated with the positive rainfall anomalies, major features in the low-level wind field include: (1) a concentrated equatorial westerly anomaly and a pair of off-equator cyclonic circulations coupling with enhanced rainfall anomalies in between propagate eastward together (2) a convergent centre that leads the maximum rainfall during the developing and mature phases and (3) a maximum westerly anomaly that lags rainfall anomalies during the developing phase but almost overlaps during the mature phase and leads the rainfall anomaly in the dissipation phase. These features have been reported by several observational studies (e.g. Rui and Wang, 1990; Jones *et al.*, 2004).

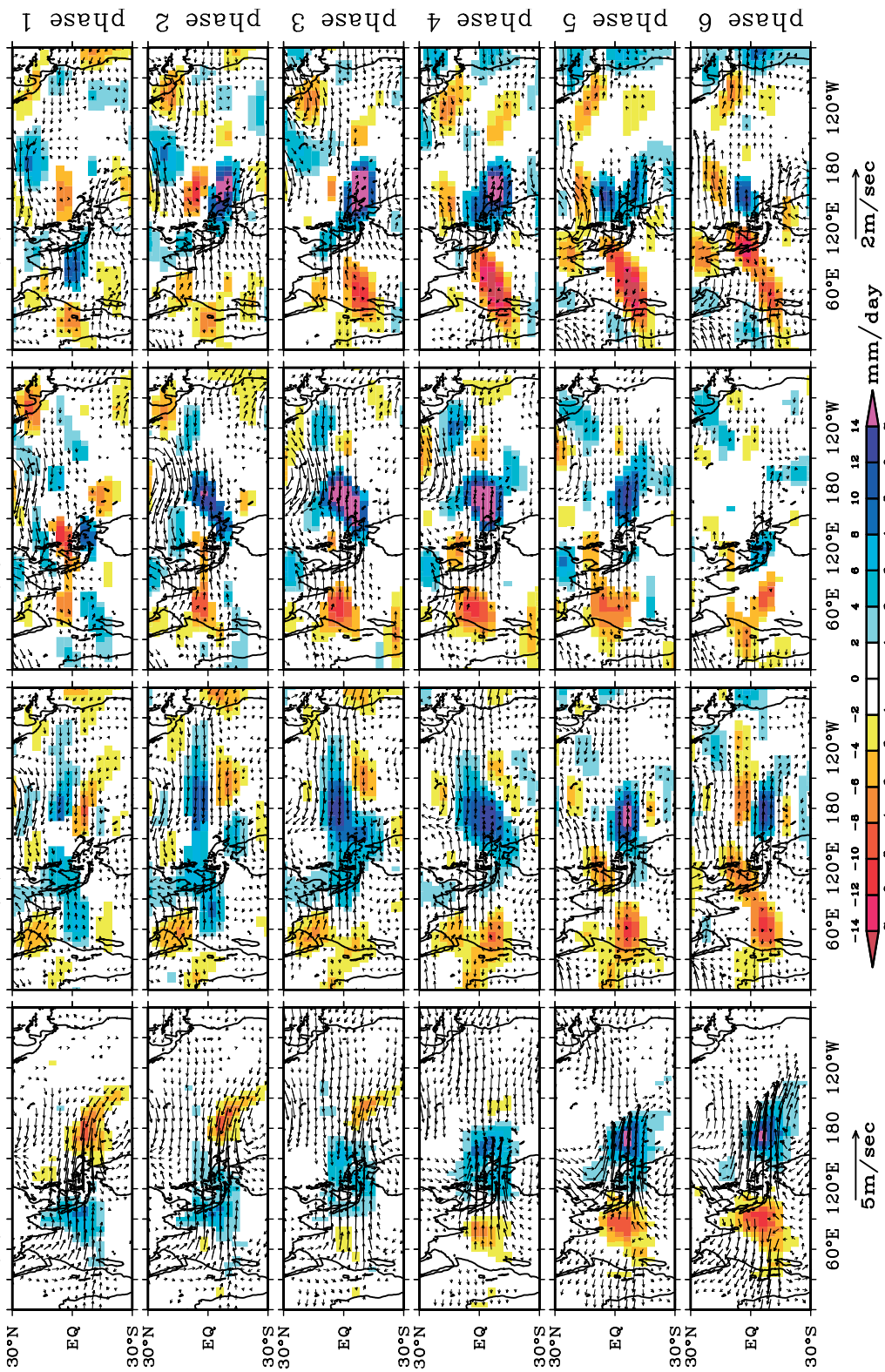

Figure 6. The ISO lifecycles in rainfall (colour-shading) and 850-mb wind (vector) anomalies composite from (a) the observations, (b) the Indo-Pacific (IP) Run, (c) the Pacific Ocean (PO) Run, and (d) the Indian Ocean (IO) Run. Only the first half of the lifecycle is shown: from phase 1 (−25 day) to phase 6 (+0 day). Only the rainfall and wind anomalies that are significant at 95% (90%) confidence level are shown. Note that the different scales are used between observed and simulated anomalies. This figure is available in colour online at www.interscience.wiley.com/ijoc

In the IP Run (Figure 6(b)), although the significant area in the tropical warm waters is smaller than the observations, the model ISO lifecycle captures many observed features well. Rainfall anomalies initiated in the equatorial Africa and propagating eastward from the Indian Ocean to the Maritime Continent are reproduced (phases 1–3). Meanwhile, the associated intensified equatorial westerly (easterly) anomalies also tend to lag the enhanced (suppressed) rainfall anomalies during this developing phase (Hendon and Salby, 1994; Zhang *et al*., 2006). Moreover, the enhanced rainfall and the lagged westerly anomalies are capable of passing through the Maritime Continent from the south and then head toward the central Pacific (phases 4–6). This run also faithfully reproduces the redevelopment of the ISO in the western Pacific warm pool (phase 3–4) and its later intersection with the SPCZ (phase 5–6). For the PO Run (Figure 6(c)), the evolution of the simulated rainfall and low-level circulation anomalies resembles that in the IP Run, with an exception that the eastward propsgation in the Indian Ocean is weaker. For the IO Run (Figure 6(d)), simulated ISO is also similar to the IP Run while travelling in the Indain Ocean sector. However, its subsequent evolution in the Pacific Ocean is very different. There exists a weaker propagating feature after the simulated ISO approaches Sumatra in phase 4. The evolutions shown in Figure 6 suggest that the ocean coupling has a stronger influence on the eastward propagation of ISO in the Pacific Ocean sector than in the Indian Ocean sector. Without the Pacific Ocean coupling, the ISO still propagates through the Indian Ocean but is weakened significantly after passing the western boundary of Pacific Ocean sector.

4. Role of ocean coupling

To understand how the ocean coupling affects the ISO propagation, we examine in Figure 7 the evolutions of the sea surface temperature anomalies (SSTA) and wind stress anomalies associated with the composite ISO lifecycle in the observations and the three CGCM runs. Note that different scales are used in the observed and simulated anomalies. In the observations, the SSTA show an eastward propagating pattern from the western Indian Ocean to the dateline. For the sake of comaparison, centres of the enhanced rainfall anomalies from Figure 6 are marked as open triangles in Figure 7(a) and (b) for the observations and the IP Run. In the observations the propagation of SSTA is in accord with that of rainfall anomalies. The enhanced rainfall anomalies are preceeded by positive SSTA and followed by negative SSTA by 2–3 pentads (Waliser *et al*., 1999; Woolnough *et al*., 2000). These phase relationships suggest that the eastward propagation of the ISO convection could be helped by the destablization effect produced by the positive SSTA to its east (Wang and Xie, 1998). The IP Run (Figure 7(b)) produces a smaller magnitude of the ISO-related SSTA than the observed. Nevertheless, the simulated SSTA still has a considerable magnitude, about 0.2°–0.3 °C. For the purpose of comparison, a smaller contour interval is used in Figure 7(b)–(d) than in Figure 7(a). In the IP Run (Figure 7(b)), SSTA propagating eastward along the equator Indian Ocean is identifiable. The anomaly centre of the SSTA is located near 70 °E in phase 1, 80 °E in phase 2, and moves to 95 °E in phase 3. This eastward propagation feature is superimposed with a standing SSTA feature centred at the 60 °E. The SSTA simulated in the IO Run (Figure 7(d)) is similar to that of the IP Run, but the eastward-propagating signal stalls as approaching the Maritime Continent. In particular, the 'accumulation' of positive SSTA in the South China Sea (phase 2–4) leads to the formation of unrealistic cyclonic anomalies (*cf* phase 4–6 in Figure 6(d)) with enhanced mean northerlies over the East Asia that reverses the polarity of anomalous SST 1 to 2 pentads later (phase 5–6).

In the Pacific Ocean, both the IP and PO Runs (Figures 7(b) and (c)) produce larger SSTA than in the Indian Ocean. The simulated SSTA has comparable magnitudes as the observations over the western Pacific warm pool and SPCZ. To the south of equator, a southeastward migration of positive SSTA capable of crossing the dateline is particularly significant in the PO Run. This would facilitate the subsequent rainfall pattern to further propagate eastward (*cf* Figure 6(c)). In the meantime, a westward signature of negative SSTA accompanied by the enhanced northeasterlies (phase 2–3) and later the easterlies (phase 5) as migrating towards New Guinea (phase 6) is also noted. Although largely masked by the dominant eastward SST signal from the Indian Ocean, footprint of this off-equator westward oceanic Rossby wave actually has its correspondence in the observation (*cf* phase 3–5 of Figure 7(a)). It features the possible interaction with the disturbances originated from the subtropics of winter hemisphere (e.g. Bladé and Hartmann, 1993) before being amplified through the air-sea coupling in the subtropical north Pacific. The phase relationships shown in Figure 7 between the simulated SST, low-level wind, and rainfall anomalies resemble the observations, suggesting that the gross features of observed ISO-SST interactions are captured by this CGCM to some extent. It is important to emphasize that the ISO-related SSTA is larger in the Pacific Ocean than in the Indian Ocean. This difference is particularly obvious in the CGCM simulations and suggests that the atmosphere-ocean coupling in the Pacific Ocean is probably more important to the ISO propagation than in the Indian Ocean.

We further analyze the surface heat fluxes associated with the composite ISO to examine how the ISO-SST interactions are produced. Figure 8 shows the composite latent heat fluxes (LHF; shadings) and short wave radiation (SWR; contours) from the observations and the three CGCM runs. The sign of the flux is positive downward. Consistent with previous studies (e.g. Woolnough *et al*., 2000), other heat flux terms are found less important to the SSTA (not shown). In the observation (Figure 8(a)), both LHF and SWR anomalies with a

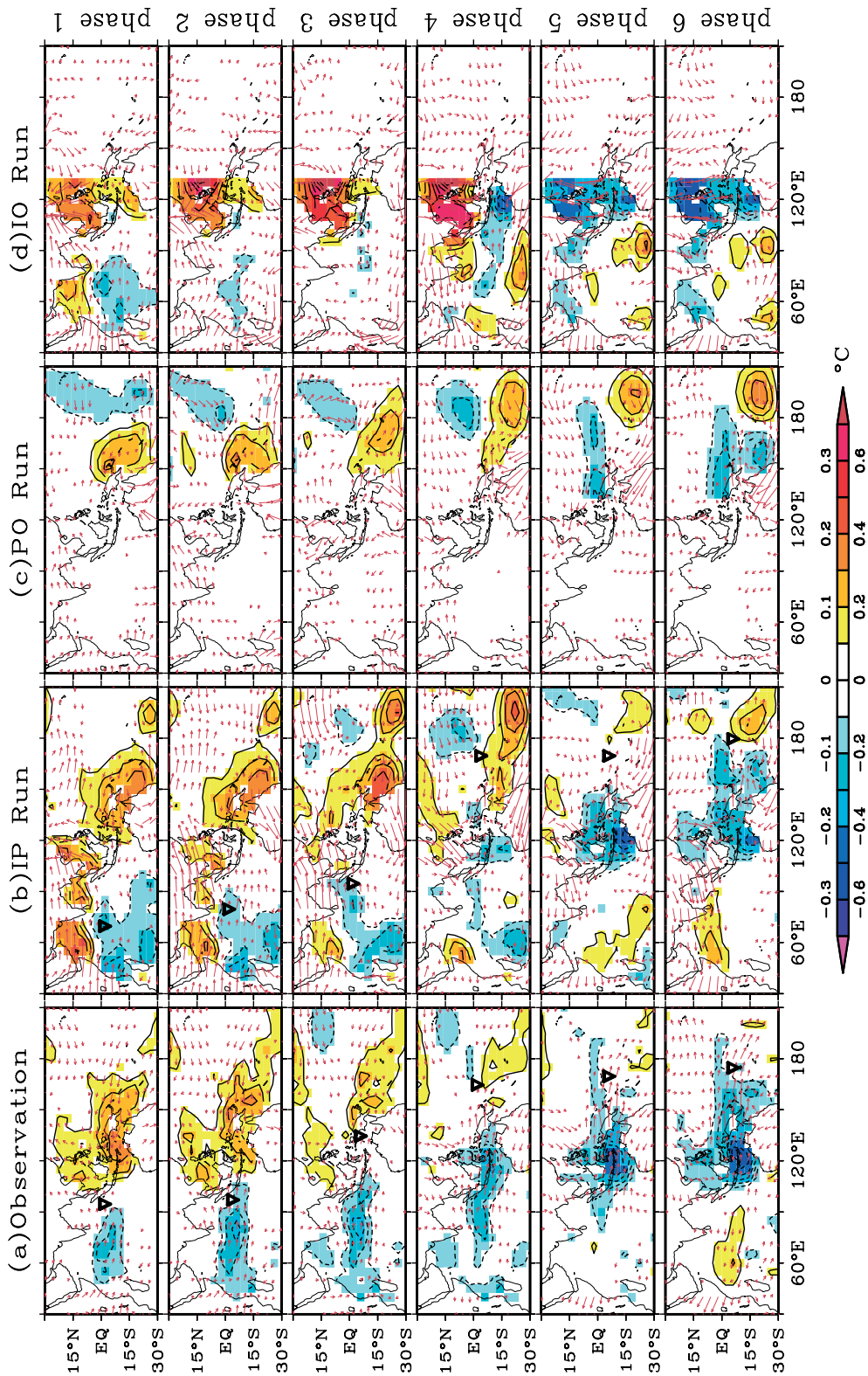

Figure 7. The ISO lifecycles in SST (colour-shading) and surface wind stress (vector) anomalies calculated from (a) the observations, (b) the Indo-Pacific (IP) Run, (c) the Pacific Ocean (PO) Run, and (d) the Indian Ocean (IO) Run. Centers of enhanced rainfall anomalies in Figures 6a and 6b are indicated as open triangles here. Note that the scale used in simulated sea surface temperature anomalies (SSTA) is only one half of that used in the observations. This figure is available in colour online at www.interscience.wiley.com/ijoc

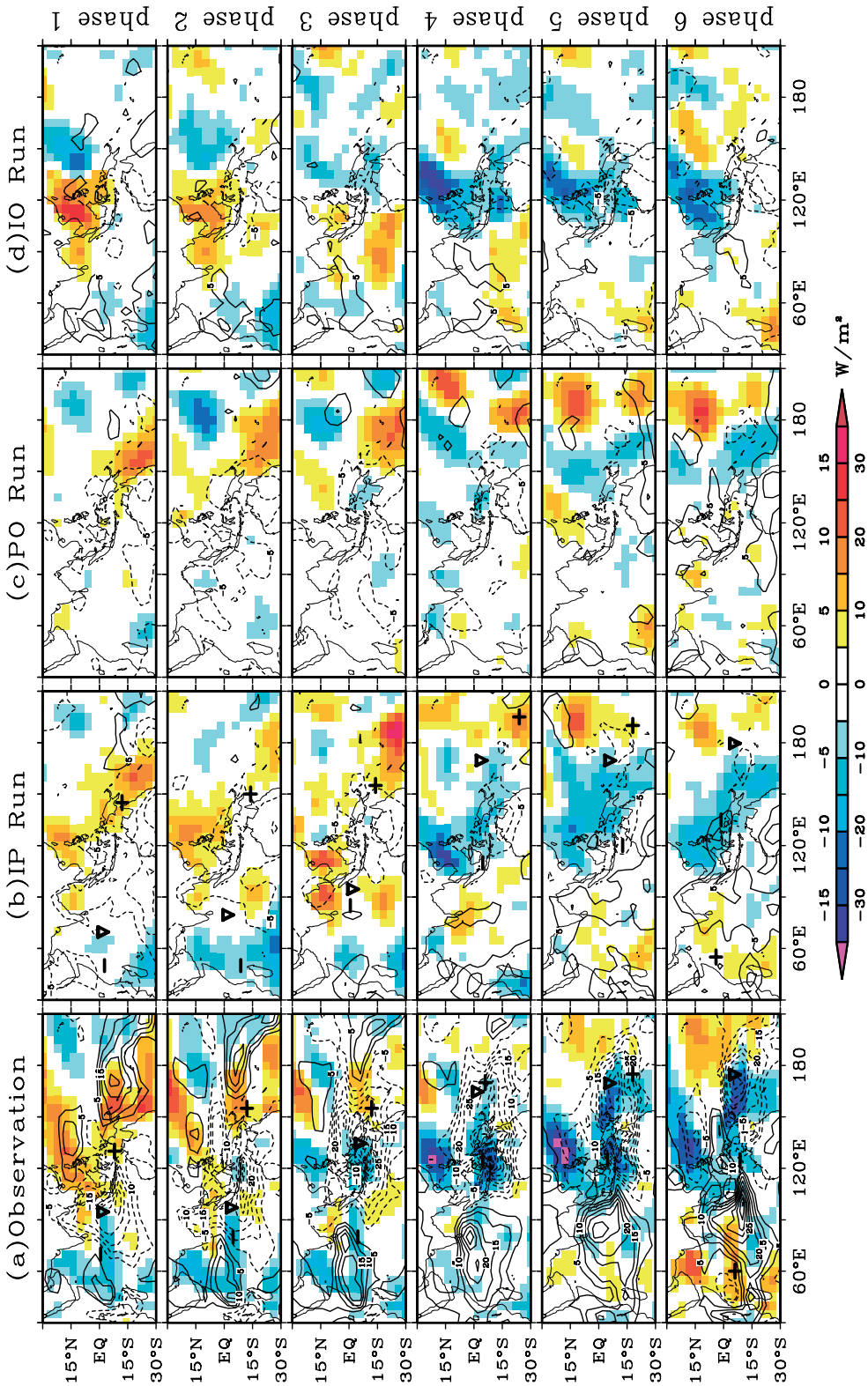

Figure 8. The ISO lifecycles in anomalous latent heat flux (LHF; colour-shading) and short-wave radiation (SWR; contour) composited from (a) the observations, (b) the Indo-Pacific (IP) Run, (c) the Pacific Ocean (PO) Run, and (d) the Indian Ocean (IO) Run. Downward fluxes are positive. Centers of enhanced rainfall and positive/negative SSTA in Figures 7a and 7b are labelled as open triangles and as +/− symbols, respectively, in panels a and b here. Note that the scale used in the simulated anomalies is only one half of that used in the observations. Contour intervals are 5 W/m^2 for (a) and 2.5 W/m^2 for (b)–(d). This figure is available in colour online at www.interscience.wiley.com/ijoc

comparable magnitude migrate eastward across the Maritime Continent and into the western Pacific. Centres of negative (reduced) SWR anomalies almost coincide with those of enhanced rainfall anomalies (open triangles) and vice versa (Inness and Slingo, 2003). As for the LHF anomalies, they have an in-quadrature phase relation with the rainfall anomalies in the region extending from the Indian Ocean to the western Pacific. Within this region, the enhanced rainfall anomalies are associated with the negative LHF anomalies (i.e. increased evaporation) to the west and positive anomalies (i.e. reduced evaporation) to the east (Woolnough *et al*., 2000; Inness and Slingo, 2003). This in-quadrature phase relation can be explained as a result of convection-wind-evaporation process. The moisture convergence induced by the convection produces westerlies to the west and easterlies to the east of the enhanced rainfall centre (see the wind vectors shown in Figure 6). Superimposed on the mean surface westerlies in the Indian Ocean and western Pacific, these wind anomalies increase wind speed to the west but decrease it to the east. Evaporation is thus enhanced to the west but weakened to the east of the enhanced rainfall centre.

The positive (negative) SSTA centre shown in Figure 7 [also marked as +(−) in Figures 8(a)–(b) for the observations and the IP Run] basically follows the centre of the positive (negative) LHF anomalies in both the Indian and Pacific oceans. It is in the western Pacific Ocean that the SWR anomalies become important to prolong the duration of SSTA. As the ISO propagates into the SPCZ and encounters the semi-permanant cloudiness, the SSTA (and thus ISO convections) disappear in response to the decaying SWR anomalies. Results of the IP Run (Figure 8(b)) indicate that the evolution of the flux terms and its lead/lag relationship with the SSTA show some resemblances with the observed large-scale features during the eastward migration of ISO. However, the simulated SWR anomalies are much smaller and less organized as compared to the LHF anomalies. Likely related to the cold biase of mean SST, these deficiencies are more serious in the Indian Ocean and western part of Maritime Continent than in the western Pacific warm pool regions. As a result, simulated SSTA appear to be mainly contributed by the LHF rather than by its collaboration with the SWR seen in observation. Same conclusion can be equally applied to both the PO Run (Figure 8(c)) and IO Run (Figure 8(d)). It is also noticed that the simulated LHF anomalies in the Indian Ocean are very small in all the three CGCM runs. The LHF anomalies are slightly larger in the IO Run. Results from Figures 7 and 8 suggest that the wind-evaporation-SST interaction is a major mechanism that allows ISO to perturb the Indo-Pacific SSTA which later helps to promote the eastward propagation of ISO. The SWR-SST interaction is another important mechanism to promote the ISO-SST interaction in the observations but is not captured by this version of the UCLA CGCM used in this study. The underestimation of the cloud-radiation-SST feedback in this model is likely due to the way cloudiness is treated in the UCLA AGCM, which is either 100% or 0%. There is no partial cloudiness in the model. As a result, the model cloudiness is not sensitive to weak ISO events and the associated shortwave radiation flux anomalies are weak.

The differences in the zonal propagation of ISO produced by the three CGCM runs could be due to the ocean coupling as well as the basic state biases produced by the coupling, such as those in SSTs. To further identify the impacts of the ocean coupling, we performed two forced AGCM runs in which the monthly SST climatologies produced by the PO and IO Runs are used as boundary conditions in the respected coupled ocean basins to drive these AGCM runs. Outside the forced ocean domains, SSTs are still prescribed by the observed monthly-mean climatology. We then contrast the ISO simulated by the forced AGCM runs with those from the basin-coupling runs. Both AGCM runs are integrated for about 13 years, and the last 10 years of the simulations are analyzed. The same EEOF and composite analyses described in Section 3 were then applied to the AGCM runs to construct the lifecycle of the simulated ISO.

Figure 9 shows the evolutions of χ'_{200} along the equator (averaged between 10 °S and 10°N) from these two AGCM runs. For the forced PO-AGCM Run (Figure 9(a)), the propagation feature still exists in the Indian Ocean which is similar to that produced in the PO Run. But the propagation feature in the Pacific Ocean is much weaker than the PO Run. The ISO anomalies with large intensities appear only to the west of 150 °E. While in the PO run (Figure 4(c)), the simulated ISO anomalies have large intensities well beyond the dateline. This difference between Figure 9(a) and Figure 4(c) suggest that the Pacific Ocean coupling can promote the ISO to propagate further into the Pacific. Results from this forced PO-AGCM Run confirm that Pacific Ocean coupling can sustain the eastward propagation of ISO. For the forced IO-AGCM Run (Figure 9(b)), the eastward propagating feature seen in the coupled IO Run is much weakened and replaced by a strong standing feature in Indian Ocean. This dramatic difference not only indicates that the Indian Ocean coupling helps the zonal ISO propagation but also suggests that the model bias in Indian Ocean SSTs causes the standing ISO oscillation around 60 °E. When observed SSTs are prescribed in the Indian Ocean, the forced PO-AGCM Run produces eastward ISO propagation without strong standing oscillation in the central Indian Ocean.

5. Summary and conclusions

In boreal winter, when warm SSTs locate mostly zonally along the equator and extend from the Indian Ocean to the central Pacific, the ISO propagation is primarily eastward. In this study, we performed basin-coupling experiments with the UCLA CGCM to examine the role of Pacific and Indian Ocean couplings in the propagation of wintertime ISO. Our modelling results show that both the Pacific and Indian Ocean couplings help

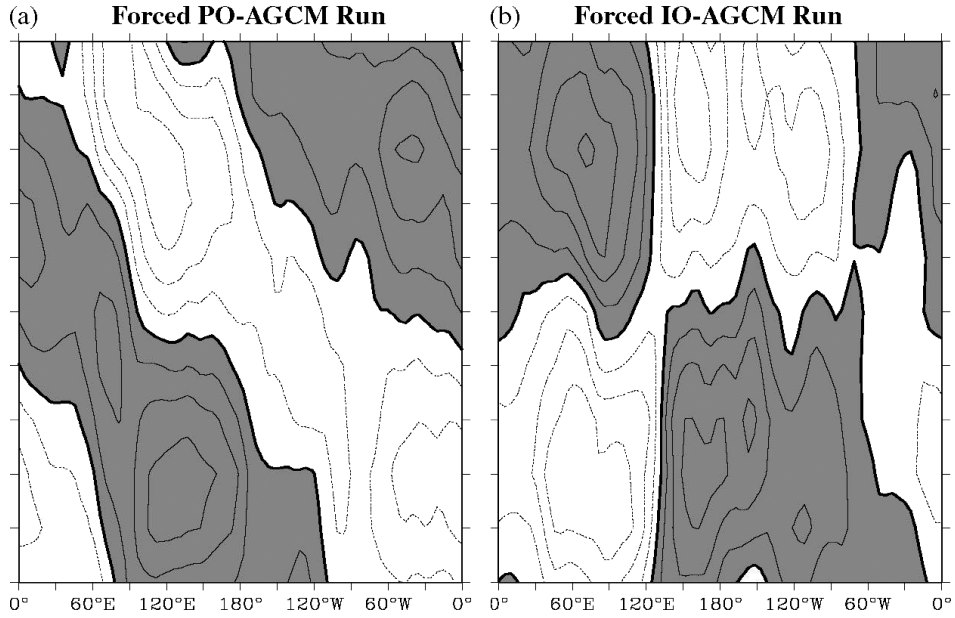

Figure 9. The lifecycles of the AGCM-simulated wintertime ISO in 200-mb velocity potential (χ'_{200}) anomalies along the equator (10 °S–10 °N). Panel (a) is composited from the forced AGCM experiment which uses the SST produced from the Pacific Ocean (PO) Run and (b) from the Indian Ocean (IO) Run. Contour intervals are $1/3 \times 10^6$ m$^2 \cdot$ sec^{-1}.

promote the ISO propagation. The Pacific Ocean coupling is particularly crucial to sustain the ISO propagation into the central Pacific. When the Pacific Ocean coupling is included, both the IP and PO Runs produce a more realistic eastward propagation. Without the Pacific Ocean coupling, the ISO simulated in the IO Run cannot propagate into the western-to-central Pacific with large intensities and is mostly confined within the Indian Ocean. The Indian Ocean coupling appear less crucial for the eastward ISO propagation. Without the Indian Ocean, the PO Run produces a weaker ISO signal in the Indian Ocean but the eastward propagation tendency still exists. The importance of ocean coupling appears increased when the ISO moves into the Pacific Ocean.

It is found that the ocean coupling promotes the ISO propagation by configuring a proper temporal and spatial phase relationship between the surface fluxes, winds, convection, and underlying SST fluctuations. In this particular CGCM, however, the ISO-related air-sea interaction is produced mainly via latent heat flux through the wind-evaporation-SST feedback. In the observations the air-sea interaction is also produced via SWR flux through the cloud-radiation-SST feedback. In the Indian Ocean, the ISO simulated by this CGCM accompanies with weaker surface heat flux and SSTA. This basin-coupling modelling study also confirms the suggestion from other studies that the extent of low-level mean westerlies near the Maritime Continent is crucial for a CGCM to have a realistic ISO simulation (e.g. Inness and Slingo, 2003; Zhang *et al*., 2006; Watterson and Syktus, 2007). We showed that such mean wind biases can be further linked to the mean SST biases and are responsible for the erroneous standing oscillations found in the central Indian Ocean and central Pacific Ocean. It should be noted that in all CGCM experiments, we can always find zonal ISO propagation in the Indo-Pacific region with or without the ocean coupling, although the propagation strength varies. It is likely that the atmospheric internal mechanisms, such as the Kelvin-Rossby wave conditional instability of the second kind (wave-CISK), alone are capable of producing the ISO propagation. But the Indian and Pacific Ocean couplings can help promote the zonal propagation in different ways. Also, the wintertime ISO variance produced by this CGCM is weak compared to the observations and, therefore, the roles of Pacific and Indian Ocean couplings concluded in this study might be changed when the ISO intensity is large enough to induce larger SSTA.

Acknowledgements

The authors thank two anomalous reviewers for their constructive comments which have improved the manuscript. The authors acknowledge the support from the National Science Council of Taiwan (NSC94-2119-M-003-004) and National Science Foundation of US (ATM-0638432). They thank Mr. Wen-Haung Huang for helping the preparation of the figures. Model simulations were performed at the University of California, Irvine's Earth System Modeling Facility (supported by NSF ATM-0321380) and the UC San Diego Supercomputer Center.

References

Bladé I, Hartmann DL. 1993. Tropical intraseasonal oscillations in a simple nonlinear model. *Journal of Atmospheric Sciences* **50**: 2922–2939.

Bryan K. 1969. A numerical method for the study of the circulation of the world ocean. *Journal of Computational Physics* **4**: 347–376.

Cox MD. 1984. *A primitive equation three-dimensional model of the ocean*. NOAA GFDL Ocean Group Technical Report No. 1, Princeton University: Princeton, NJ; 75 pp.

Fraedrich K, McBride JL, Frank WM, Wang R. 1997. Extended EOF analysis of tropical disturbances: TOGA COARE. *Journal of Atmospheric Sciences.* **19**: 2363–2372.

Fu X, Wang B. 2004. Differences of boreal-summer intraseasonal oscillations simulated in an atmosphere-ocean coupled model and an atmosphere-only model. *Journal of Climate* **17**: 1263–1271.

Hannachi A, Jolliffe IT, Stephenson DB. 2007. Empirical orthogonal functions and related techniques in atmosphere sciences: A review. *International Journal of Climatology* DOI: 10.1002/joc.1499.

Hendon HH, Glick J. 1997. Intraseasonal air–sea interaction in the tropical Indian and Pacific Oceans. *Journal of Climate* **10**: 647–661.

Hendon HH, Salby ML. 1994. The lifecycle of the Madden–Julian oscillation. *Journal of Atmospheric Sciences* **51**: 2225–2237.

Inness PM, Slingo JM. 2003. Simulation of the Madden–Julian oscillation in a coupled general circulation model. Part I: Comparison with observations and an atmosphere-only GCM. *Journal of Climate* **16**: 345–364.

Jones C, Carvalh LMV, Higgins RW, Waliser DE, Schemm JKE. 2004. Climatology of tropical intraseasonal convective anomalies 1979–2004. *Journal of Climate* **17**: 523–539.

Krishnamurti TN, Osterhof DK, Mehta AV. 1988. Air–sea interaction on the time scale of 30–50 days. *Journal of Atmospheric Sciences* **45**: 1304–1322.

Lau KM, Sui CH. 1997. Mechanisms for short-term sea surface temperature regulation: Observations during TOGA COARE. *Journal of Climate* **10**: 465–472.

Madden RA, Julian PR. 1971. Detection of a 40–50 day oscillation in the zonal wind in the tropical Pacific. *Journal of Atmospheric Sciences* **28**: 702–708.

Madden RA, Julian PR. 1972. Description of global-scale circulation cells in the tropics with a 40–50 day period. *Journal of Atmospheric Sciences* **29**: 1109–1123.

Mechoso CR, Yu JY, Arakawa A. 2000. A coupled GCM pilgrimage: From climate catastrophe to ENSO simulations. *General Circulation Model Development: Past, Present, and Future*, Randall DA (ed). Academic Press: London; 539–575.

Reynolds RW, Rayner NA, Smith TM, Stokes DC, Wang W. 2002. An improved in situ and satellite SST analysis for climate. *Journal of Climate* **15**: 1609–1625.

Rui H, Wang B. 1990. Development characteristics and dynamic structure of tropical intraseasonal convection anomalies. *Journal of Atmospheric Sciences* **47**: 357–379.

Uppala SM, Kållberg PW, Simmons AJ, Andrae U, da Costa Bechtold V, Fiorino M, Gibson JK, Haseler J, Hernandez A, Kelly GA, Li X, Onogi K, Saarinen S, Sokka N, Allan RP, Andersson E, Arpe K, Balmaseda MA, Beljaars ACM, van de Berg L, Bidlot J, Bormann N, Caires S, Chevallier F, Dethof A, Dragosavac M, Fisher M, Fuentes M, Hagemann S, Hólm E, Hoskins BJ, Isaksen L, Janssen PAEM, Jenne R, McNally AP, Mahfouf JF, Morcrette JJ, Rayner NA, Saunders RW, Simon P, Sterl A, Trenberth KE, Untch A, Vasiljevic D, Viterbo P, Woollen J. 2005. The ERA-40 re-analysis. *Quarterly Journal of the Royal Meteorological Society* **131**: 2961–3012.

Waliser DE, Lau KM, Kim JH. 1999. The influence of coupled SSTs on the Madden–Julian oscillation: A model perturbation experiment. *Journal of Atmospheric Sciences* **56**: 333–358.

Wang B. 2005. Theory. *Tropical Intraseasonal Oscillation in the Atmosphere and Ocean*, Lau William K-M, Waliser DE (eds). Praxis Publishing Ltd.: Chichester, UK; 307–360.

Wang B, Fan Z. 1999. Choice of South Asian summer monsoon indices. *Bulletin of the American Meteorological Society* **80**: 629–638.

Wang B, Rui H. 1990. Synoptic climatology of transient tropical intraseasonal convection anomalies. *Meteorology and Atmospheric Physics* **44**(1–4): 43–61.

Wang B, Xie X. 1998. Coupled modes of the warm pool climate system Part I: The role of air-sea interaction in maintaining Madden-Julian oscillation. *Journal of Climate* **11**: 2116–2135.

Watterson IG. 2002. The sensitivity of subannual and intraseasonal tropical variability to model ocean mixed layer depth. *Journal of Geophysical Research* **107**: DOI 10.1029/2001JD000671.

Watterson IG, Syktus J. 2007. The influence of air-sea interaction on the Madden-Julian Oscillation: the role of seasonal mean state. *Climate Dynamics* **28**: DOI 10.1007/s00382-006-0206-9.

Weare BC, Nasstrom JS. 1982. Examples of extended empirical orthogonal functions. *Monthly Weather Review* **110**: 481–485.

Weller RA, Anderson SP. 1996. Surface meteorology and air-sea fluxes in the western equatorial Pacific warm pool during the TOGA coupled ocean-atmosphere response experiment. *Journal of Climate* **9**: 1959–1990.

Wheeler MC, Hendon HH. 2004. An all-season real-time multivariate MJO index: Development of an index for monitoring and prediction. *Monthly Weather Review* **132**: 1917–1932.

Woolnough SJ, Slingo JM, Hoskins BJ. 2000. The relationship between convection and sea surface temperature on intraseasonal timescales. *Journal of Climate* **13**: 2086–2104.

Xie P, Arkin PA. 1997. Global precipitation: A 17-year monthly analysis based on gauge observations, satellite estimates, and numerical model outputs. *Bulletin of the American Meteorological Society* **78**: 2539–2558.

Yu JY, Mechoso CR. 2001. A coupled atmosphere-ocean GCM study of the ENSO cycle. *Journal of Climate* **14**: 2329–2350.

Zhang C. 1996. Atmospheric intraseasonal variability at the surface in the tropical western Pacific Ocean. *Journal of Atmospheric Sciences* **53**: 739–758.

Zhang C. 1997. Intraseasonal variability of the upper-ocean thermal structure observed at 0° and 165°E. *Journal of Climate* **10**: 3077–3092.

Zhang C, Dong M, Gualdi S, Hendon HH, Maloney ED, Marshall A, Sperber KR, Wang W. 2006. Simulations of the Madden-Julian oscillation in four pairs of coupled and uncoupled global models. *Climate Dynamics* **27**: 573–592.

